mathematics

MDPI

Article

Complex Dynamical Sampling Mechanism for the Random Pulse Circulation Model and Its Application

Lin Tang [1,2,3,4], Kaibo Shi [1,*] and Songke Yu [1]

[1] College of Electronic Information and Electrical Engineering, Chengdu University, Chengdu 610106, China
[2] National Engineering Research Center for Agro-Ecological Big Data Analysis & Application, Anhui University, Hefei 230039, China
[3] Guangxi Key Lab of Multi-Source Information Mining & Security, Guangxi Normal University, Guilin 541004, China
[4] Data Recovery Key Laboratory of Sichuan Province, College of Mathematics and Information Science, Neijiang Normal University, Neijiang 641100, China
* Correspondence: skbs111@163.com

Abstract: The fast multi-pulse spectrum is a spectrum acquisition method that obtains an average pulse amplitude in a dynamic window, which improves the energy resolution by sharpening peaks in the acquired spectra, but produces the counting loss. Owing to the counting loss problem, a counting rate multiplication method based on uniform sampling, also called the pulse circulation method, is presented in this paper. Based on the theory of mathematical statistics and uniform sampling, this method adopted a dynamic sample pool to update the pulse amplitude sample in real time. Random numbers from the uniform distribution were sampled from the sample pool, and the sampled results were stored in the random pulse circulator so that the pulse amplitude information used for spectrum generation was uniformly expanded. In the experiment section, the obtained spectrum was analyzed to verify the multiplication effect of the pulse circulation method on the counting rate and the compensation effect of the fast multi-pulse spectrum algorithm on the counting rate loss. The results indicated that the characteristic peaks of each element in the X-ray spectrogram obtained by the pulse circulation method could realize counting rate multiplication uniformly, and the multiplication ratio of every element was approximately equal. This is of great significance for obtaining an accurate X-ray fluorescence spectrum.

Keywords: X-ray spectrogram; dynamic sample pool; counting rate multiplication; random pulse circulator

MSC: 62-08

Citation: Tang, L.; Shi, K.; Yu, S. Complex Dynamical Sampling Mechanism for the Random Pulse Circulation Model and Its Application. *Mathematics* **2023**, *11*, 668. https://doi.org/10.3390/math11030668

Academic Editors: Xinsong Yang and Ruofeng Rao

Received: 15 December 2022
Revised: 16 January 2023
Accepted: 17 January 2023
Published: 28 January 2023

1. Introduction

X-ray fluorescence spectroscopy is a well-known analytical technique that has gained significant analytical prominence in the last 20 years; it has been applied widely in several fields, and spectrum analysis technology is also developing [1–3]. The two most important indicators in X-ray measurement are energy resolution and counting rate, which are contradictory. Usually, improving the energy resolution will reduce the counting rate, while increasing the counting rate will give rise to losing the energy resolution. The detector's energy resolution is determined by several factors, such as the statistical fluctuation of the detected signal, noise of the signal processor, external interference and temperature, and so on. Statistical fluctuations determine the theoretical limits of the given detector's energy resolution, and the effects of other factors can be reduced by appropriate noise filtering and electronic techniques [4–7].

The main objective of the X-ray fluorescence spectroscopy is to record a spectrum from a detector, and a traditional method of recording a spectrum is a multichannel pulse height analyzer (MCA), whose main feature is that the increment of the count on each channel is

based on the single pulse amplitude, that is, a simple single pulse spectrum (SSPS) [8]. As for the elements with low content, the counting rate is low, and therefore, their spectrum is greatly impacted by the statistical fluctuation, and the repeatability of the measurement result is not satisfactory. Another improved spectral method is the fast multi-pulse spectrum (FMPS) acquisition method that averages pulse heights in dynamic windows and sharpens characteristic peaks in the acquired spectra. Our team members have applied for invention patents for this technology [9,10]. In view of the limited space, this paper focuses on the improving the effect of the pulse circulation method on the counting rate and the statistical test after using the pulse circulation method. More detailed derivation and implementation of FMPS technology will be published in subsequent papers. Preliminary experiments demonstrated that the FMPS method had a higher energy resolution than the SSPS method, but at the same time, it also had the defect of counting rate loss.

The preliminary research [11–13] has put forward the pulse rejecting method and pulse repair method, which can lend a great hand to deal with the abrupt pulse and obtain real and reliable pulse amplitude information. At present, the application of FMPS mainly solves two kinds of problems. The first problem is to predict the contents of elements and compounds of substances or other quantities of substances. Another problem is to predict the type of substance or other labels of substances. The application of FMPS could improve the accuracy of content analysis and the composition analysis of the substance. There are also some problems and challenges in FMPS algorithms, such as counting loss.

To solve the counting loss produced by FMPS [14], this paper proposes a pulse circulation method for multiplying the counting rate. This method is based on mathematical statistics, and a new pulse amplitude sequence is formed by random sampling in the original pulse amplitude sequence [15–18]. Additionally, the new sequence must keep the statistical characteristics of the original pulse amplitude sequence. The difference between the pulse circulation method and the conventional spectrum construction method is that the former multiplies the number of pulse amplitude samples by uniform sampling to compensate for the loss of the number of amplitude samples caused by the average window amplitude of the FMPS method. The results show that the pulse circulation method can effectively solve the counting rate loss caused by the FMPS method.

2. Principle

The pulse circulation method's key is adding a sample pool and a random pulse circulator (RPC). The sample pool stores the pulse amplitude information, whose maximum capacity is L. The random number generator is used to generate random numbers X_i, which obeys uniform distribution (X_i~U) and takes a value in the interval of [1, L]. The X_ith pulse amplitude information in the sample pool is taken out and stored in the RPC. The capacity of the RPC is set to N, whose first pulse amplitude is always the original pulse sequence without sampling, while the next $N - 1$ pulse amplitude sample is the multiplication pulse sequence sampled by the random number X_i in the sample pool. N pulse amplitudes enter the FPGA (field-programmable gate array) to complete multichannel pulse spectroscopy by the FMPS method. Based on the sample pool, random number generator, RPC, and first in, first out (FIFO) arrays, the pulse circulation method ingeniously enlarges the number of samples without introducing more noise, effectively increasing the counting rate and reducing the statistical fluctuation. The schematic diagram of energy spectrum multiplication technology is shown in Figure 1.

In this figure, CLK represents the system clock, and the clock frequency must be greater than the frequency of the random number generator generating a random number. For example, when the system clock is 20 MHz, a frequency less than 20 MHz can be selected as the sampling frequency for the samples in the sample pool, but the relationship between the frequency and the system clock frequency must be an integral multiple.

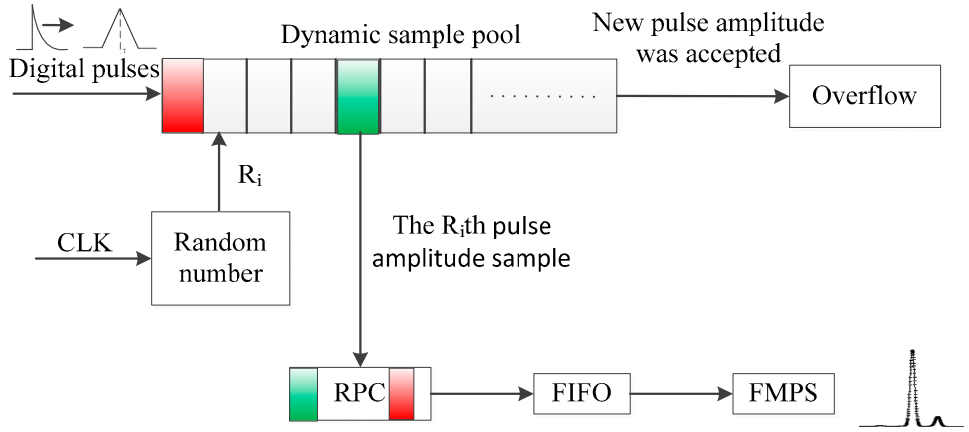

Figure 1. Counting rate multiplication principle.

3. Method

3.1. Random Number

The decay of radionuclides is random in time, and the characteristics of nuclear signals vary in time and amplitude. Yu Guogang [19] described in detail the distribution characteristics of nuclear signals in a time interval and an amplitude and concluded that the nuclear pulses of single energy usually conform to the normal distribution in amplitude, while the statistical characteristics are approximately distributed exponentially in the time interval.

In this paper, a new spectral measurement method was proposed. Firstly, this method identified and digitized the nuclear pulse amplitudes [20] and stored the digitized nuclear pulse amplitude information in the sample pool. Then, the random number Xi produced by the random number generator was used for sampling in the sample pool, and the sampling results were stored in the RPC for the next processing of FPGA. Ideally, when the size of the sample pool is large enough, or a dynamic sample pool is used, as long as the random number generated is uniform enough, the content on each channel should increase synchronously, and the statistical characteristics should be the same as those of the original spectrum. In practical applications, the generation of random numbers is implemented by FPGA, which generates several random variables in the specified sample space and ensures that all random variables have the same probability at any point in the sample spaces. In other words, we need the probability density function values of all random variables to be equal in the sample spaces.

Obviously, these random numbers' probability density coincides with the uniform distribution characteristics. No matter how large the sample space and the sample number of random variables are, the probability of the random variables subject to uniform distribution at any point in the sample space must be the same. Therefore, the final choice of the pulse circulation method was a random number generator with uniform distribution.

In probability theory and statistics, uniform distribution is also called rectangular distribution, and its probability distribution is symmetrical, that is to say, the probability distribution in the same-length region is equal. For X~U(a,b), it contains two parameters, a and b, which represent the minimum and maximum values of an interval on the axis of numbers, respectively.

The density function of random variable X is defined as:

$$f(x) = \begin{cases} \frac{1}{b-a}, & a \le x \le b \\ 0, & \text{other} \end{cases} \quad (1)$$

This paper defined the sample space as 1~4096, and we concluded that X~U [1, 4096]. To verify whether the 4096 random numbers satisfied the uniform distribution, this paper obtained the density function graph through the probability density function pdf (name,

x, A, B). Here, the name of the pdf (name, x, A, B) function was unified. A and B took 1 and 4096, respectively. According to the definition of the uniform distribution probability density function, it was easy to calculate the probability density function in the sample space of [1, 4096], whose value was 1/4095, so the probability density function graph of the uniform distribution was obtained, as shown in Figure 2.

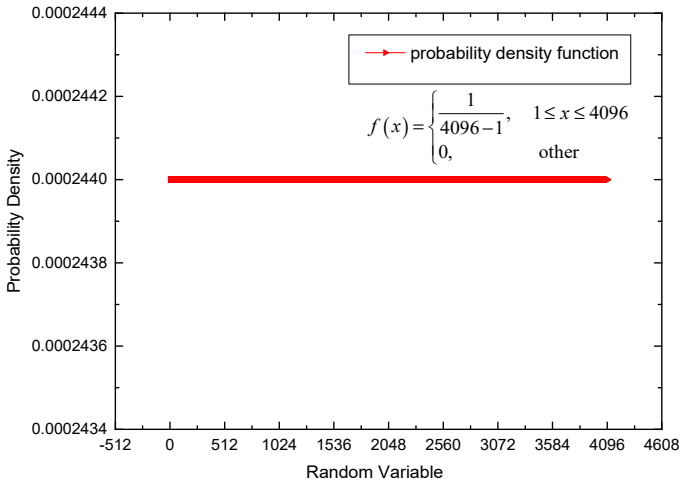

Figure 2. The probability density function of uniform distribution.

3.2. Sample Pool

In this paper, the sampling with replacement was used for the discrete sequence constituted by nuclear pulse amplitude. We assumed that the sample pool capacity was fixed to L, the information of each pulse amplitude in the sample pool was the discrete random variable X, and the value of each random variable taken from the sample pool was $X_i(i = 1, 2, 3, \dots)$. Therefore, the probability of taking out any random variable can be expressed as $P(X = X_i) = P_i(i = 1, 2, 3, \dots)$, where $P_i > 0$, $\sum_{i=1}^{L} P_i = 1$.

The sampling process is described as follows:

(1) The random number generator generated a random integer i, i~U [1, L].
(2) Because the capacity of the sample pool was fixed to L, the value of L was 4096 in this paper. The random variables needed for sampling must be the random numbers in the interval of [1, 4096].
(3) Pulse amplitude in the sample pool was sampled, and the sampled pulse amplitude was recorded as X_i.
(4) Repeated sampling.

In random sampling, the probability of the random variable $X = X_i$ (i = 1, 2, 3 ...) was $P_i(0 < P_i < 1)$. In each random sampling, the probability of $X = X_i$ was unchanged, and the results of each random sampling were independent of the other random samplings. Therefore, we judged that the result of the single random sampling $X = X_i$ was a Bernoulli test. If the probability of event A ($X = X_i$) occurrence is defined as p, and the number of occurrences is n_A, then n_A obeys the binomial distribution with parameters n and p. We mentioned that X_1, X_2, X_3, X_4, ..., X_n were n-independent random variables that obey the 0–1 distribution with parameter p. The expectation and variance of the binomial distribution were represented by $E(X_i)$ and $D(X_i)$, respectively.

Here, $n_A = \sum_{i=1}^{L} X_i$.

$$\begin{cases} E(X_i) = p \\ D(X_i) = p(1-p) \end{cases}, i = 1, 2, 3, \dots, n.$$

For any,

$$\begin{aligned}\lim_{n\to+\infty} P\left(\left|\frac{n_A}{n}-p\right|<\varepsilon\right) &= \lim_{n\to+\infty} P\left(\left|\frac{\sum_{i=1}^{n} X_i}{n}-E(X_i)\right|<\varepsilon\right)\\ &= \lim_{n\to+\infty} P\left[\left|\frac{\sum_{i=1}^{n} X_i}{n}-E\left(\frac{\sum_{i=1}^{n} X_i}{n}\right)\right|<\varepsilon\right]\end{aligned} \tag{2}$$

From Formula (2), it can be concluded that:

$$\begin{aligned}\lim_{n\to+\infty} P\left[\left|\frac{\sum_{i=1}^{n} X_i}{n}-E\left(\frac{\sum_{i=1}^{n} X_i}{n}\right)\right|<\varepsilon\right] &\geq \lim_{n\to+\infty}\left[1-D\left(\frac{\sum_{i=1}^{n} X_i}{n}\right)/\varepsilon^2\right]\\ &= \lim_{n\to+\infty}\left[1-\frac{\sum_{i=1}^{n} D(X_i)}{(n\varepsilon)^2}\right]\\ &= \lim_{n\to+\infty}\left[1-\frac{p(1-p)}{(n\varepsilon)^2}\right]=1\end{aligned} \tag{3}$$

In addition:

$$\lim_{n\to+\infty} P\left[\left|\frac{\sum_{i=1}^{n} X_i}{n}-E\left(\frac{\sum_{i=1}^{n} X_i}{n}\right)\right|<\varepsilon\right]\leq 1 \tag{4}$$

From Formulas (3) and (4), it can be concluded that:

$$\lim_{n\to+\infty} P\left[\left|\frac{\sum_{i=1}^{n} X_i}{n}-E\left(\frac{\sum_{i=1}^{n} X_i}{n}\right)\right|<\varepsilon\right]=1 \tag{5}$$

The simplified results of Formula (5) are as follows:

$$\lim_{n\to+\infty} P\left(\left|\frac{n_A}{n}-p\right|<\varepsilon\right)=1 \tag{6}$$

Formula (6) shows that when the number of extractions n was large enough, the ratio of the number of occurrences of event A to the total number of samples was closer to the probability of the occurrence of event A. To further verify this formula, this paper assumed that the estimation value of event occurrence probability, $\hat{p}$, could be calculated, as shown in Formula (7).

$$\hat{p}=\frac{n_A}{n} \tag{7}$$

As previously stated, if the probability of event A ($X = X_i$) occurrence is defined as p, and the number of occurrences is n_A, then n_A obeys the binomial distribution with parameters n and p.

$$E\left(\frac{\mathrm{n}_A}{\mathrm{n}}\right)=E(\hat{p})=E\left(\frac{\sum_{i=1}^{n} X_i}{\mathrm{n}}\right)=E(\mathrm{p})=p \tag{8}$$

Therefore, $\hat{p}$ is the unbiased estimate of p.

$$D(\hat{p}) = D\left(\frac{n_A}{n}\right) = D\left(\frac{\sum_{i=1}^{n} X_i}{\mathrm{n}}\right) = \frac{D\left(\sum_{i=1}^{n} X_i\right)}{n^2} = \frac{\sum_{i=1}^{n} D(X_i)}{n^2} = \frac{D(X_i)}{n} = \frac{p(1-p)}{n} \tag{9}$$

It was concluded that the larger the sampling number n, the closer the estimated value $\hat{p}$ was to the theoretical value p. In order to make the sampling number n large enough, the capacity of the sample pool needed to be as large as possible, but the capacity of the sample pool was restricted by hardware. Therefore, this paper used a dynamic sample pool with a capacity of 4096 to simulate an infinite sample pool by updating the sample information in the sample pool in real time.

Unlike the static sample pool, the dynamic sample pool did not need a large capacity. The most important feature of the dynamic sample pool was real-time updating. It was designed as a FIFO, with a fixed size of 4096, and always kept FIFO at full load. Every time a new pulse amplitude sample entered, the first sample would be overflowed in FIFO to ensure that the samples in the dynamic sample pool were updated in real time, which better guaranteed the randomness of the samples taken from the sample pool.

3.3. Random Pulse Circulator

In this paper, the N pulse amplitude samples stored in the RPC could be divided into two kinds of pulse sequences, called original pulse sequence and sampling pulse sequence. All pulse amplitudes entered the RPC as the original pulse sequence directly. At the same time, the pulse amplitudes were stored in a dynamic sample pool. In this paper, the remaining $N - 1$ samples in the RPC were sampled, which was called the sampling pulse sequence. As mentioned above, each sample pool had L linearly addressable cells. When the dynamic sample pool was used, the value of L was 4096.

The working principle of RPC is shown in Figure 3. The random number generator outputs the random variable $\mathrm{R_i}$ as a channel address to address a storage unit in the sample pool. R_i~U [1, 4096], and therefore, the probability that each sample is addressed in the sample pool is the same. The RPC consisting of the original pulse sequence and the sampling pulse sequence will increase the number of samples used to form the spectrum. The sample multiplication's influence on the spectrum's counting rate will be verified by simulation and experimentation, respectively.

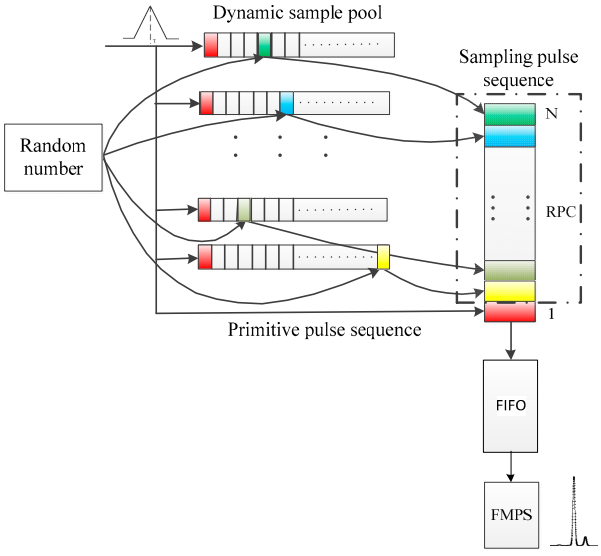

Figure 3. Working principle of the RPC.

3.4. Implementation Process

As mentioned above, the implementation of the pulse cycling method was based on a sample pool, random number generator, and random pulse circulator, and its implementation process is described below. The analog-to-digital conversion unit composed of high-precision ADC (analog-to-digital converter) first converted the collected negative exponential pulse signal sequence into the discrete pulse amplitude sequence. Then, it took out the amplitude of the forming result after completing digital pulse forming. Each pulse amplitude was taken as the second value. A pulse sequence directly entered the RPC and then judged whether the sample pool was full. If it was full, it needed to overflow and then store the new sample amplitude into the sample pool to form a second pulse sequence. The essence of the first pulse sequence was the original pulse sequence. Each pulse amplitude sample, when stored in the sample pool, was stored in the random pulse circulator as the first pulse sequence. The essence of the second pulse sequence was the random combination of $n-1$ first pulse sequences. The random number generator generated the random variable X_i (X_i~U) and then generated the random variable X_i in the sample pool. The pulse amplitude information of the storage unit corresponding to X_i was extracted from the pool and stored in the random pulse circulator. Finally, the corresponding spectrum was obtained according to all the pulse amplitude information entering the random pulse circulator. The pulse amplitude information used for forming was increased by N times, and the counting rate was also increased correspondingly.

4. Simulation

Li Dongcang [21] obtained pseudo-random numbers R (R~U), as shown in Formula (10).

$$R(i) = 0.5 - Rnd(1) \tag{10}$$

$Rnd(1)$, as a random function, generated a pure decimal number greater than 0 but less than 1. Based on Formula (10), the random sequence $X(k)$ of obeying uniform distribution and the sample sequence $Y(k)$ of obeying normal distribution were obtained. The normal distribution diagram is shown in Figure 4.

$$\begin{cases} X(k) = 200 \times \sum_{i=1}^{i=24} R(i) \\ Y(k) = 1000 + X(k)/24 \end{cases} \tag{11}$$

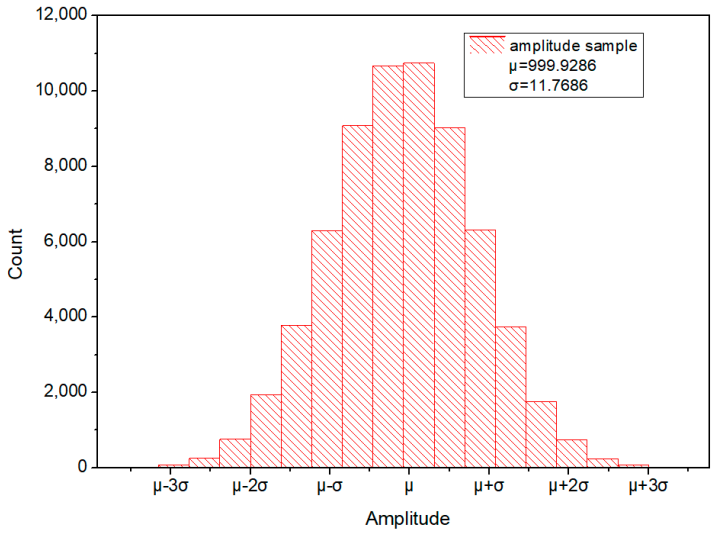

Figure 4. Normal distribution of amplitude samples.

Figure 4 contains 65,536 amplitude samples calculated using Formula (11). Here, $1 \leq k \leq 65{,}536$. On this basis, the average sample amplitude μ was 999.9286, and the standard deviation σ was 11.7686. The normal distribution of samples is shown in Figure 4.

According to the nature of normal distribution, more than 99% of the amplitude samples were distributed in 3σ intervals, and all of them were located in the [952, 1054] interval.

Taking 65,536 pulse amplitudes shown in Figure 4 as sample pools, because the range of the sample amplitude was small, a simple multichannel spectral algorithm was used to obtain the multichannel spectrum. One-half of the sample amplitude was taken as the corresponding channel address, and the counting on the corresponding channel address was added. The multichannel spectrum generation algorithm, Algorithm 1, was implemented by calling the Visual Basic macro function in Excel, where column N stored multichannel spectrum data generated by 65,536 amplitude samples randomly selected, and the channel address was 1024. Column O stored 65,536 amplitude samples specified from column L by random numbers obeying uniform distribution within the interval [1, 65,536]. Column L stored 65,536 numbers in the [960–1040] interval that obeyed the normal distribution.

The spectrum obtained by calling Algorithm 1 is shown in Figure 5a. C_{peak} expressed the peak value of the counting rate, and its value was 4407. It can be concluded that the energy resolution of the spectrum line can be expressed by FWHM (full-width at half maximum), and the FWHM was 14.

Algorithm 1 Multichannel spectrum generation algorithm

```
Sub Macro ()
Dim a, b, rc, rc2 As Single
Dim index As Integer
For i = 1 To 1024
    tt = 0
    ss = "N" + Format(i)
    Range(ss).Value = tt
Next i
peak = 0
For i = 1 To 65536
    ss = "O" + Format(i)
    tt = Range(ss).Value
    index = tt / 2
    ss = "N" + Format(index)
    tt1 = Range(ss).Value + 1
    Range(ss).Value = tt1
Next i
End Sub
```

Taking the 65,536 pulse amplitudes shown in Figure 5 as sample pools, 4 × 65,536 random numbers were generated, which obeyed uniform distribution in the interval (1, 65,536); the amplitudes in the sample pool were sampled, and a new sequence of the amplitude sample was obtained. Its multichannel spectrum is shown in Figure 5b. C_{peak}, the peak value of the counting rate, equaled 17,762.

Although the C_{peak} in Figure 5b is not equal to four times the C_{peak} in Figure 5a, the sum of counting on the whole spectrum was always equal to four times the total spectrum counting sum in Figure 5a. The FWHM of the spectral lines is equal to 14 in Figure 5a, consistent with Figure 5b.

The above simulation results showed that when the sample pool remained unchanged but the sampling times increased to four times, the peak value of the counting rate increased about four times, correspondingly, and the sum of the multiplication counting rate must be equal to four times the sum of the original counting rate on the whole spectrum. In addition, the FWHM, which represents the energy resolution of the spectral lines, remained unchanged before and after multiplication.

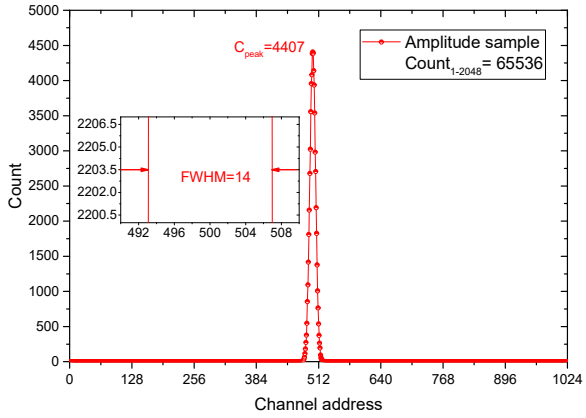

(**a**)

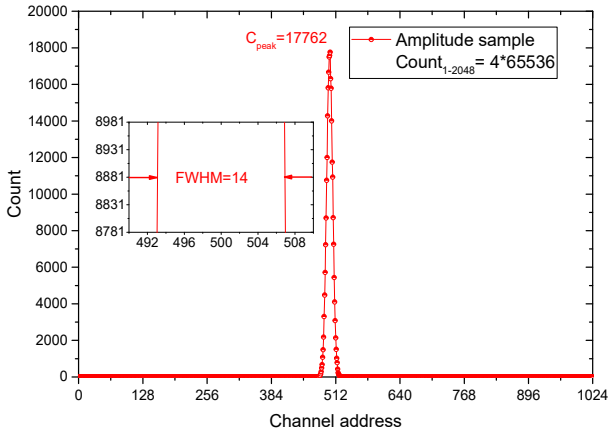

(**b**)

Figure 5. Spectral contrast maps obtained before and after multiplication. (**a**) Original spectrum; (**b**) multiplication spectrum.

The above simulation results aimed at a simple single peak and single component, which was not enough to prove that this method can effectively achieve the multiplication of the counting rate in practical application. In the next section, we use the amplitude sample measured by the actual sample as the sample pool to compare the multiplied spectrum with the original spectrum.

5. Experiment Results

In the experimental verification, we used a fast silicon drift detector as the detector, with a collimated active area of 25 mm^2, detector thickness of 500 mm, and Be window thickness of 0.5 mil. The Ag target was selected as the anode target, and the excitation source was a KYW2000A X-ray tube with a rated tube voltage of 50 kV and a rated tube flow of 0–1 mA. In the measurement process, the pulse time constant was set to 3.2 ms, with an ADC sampling frequency of 20 MHz, a sampling period of 50 ns, and a measurement time of 120 s. Based on the above experimental platform, the spectra obtained by the pulse circulation method, by FMPS, and by the superimposing pulse circulation method on the FMPS algorithm were analyzed with the same sample, respectively, to verify the multiplication effect of the pulse circulation method on the counting rate and the compensation effect on the counting loss caused by the FMPS algorithm.

5.1. Pulse Circulation Method

In order to better verify the multiplication of the element counting rate in each energy band, the self-made samples were used in the experiment. Two spectra were obtained in

the same measuring time before and after the multiplication method. As shown in Figure 6, the sample's main elements were iron, strontium, and tin, whose element symbols can be represented as follows: Fe (Ferrum), Sr (Strontium), and Sn (Stannum).

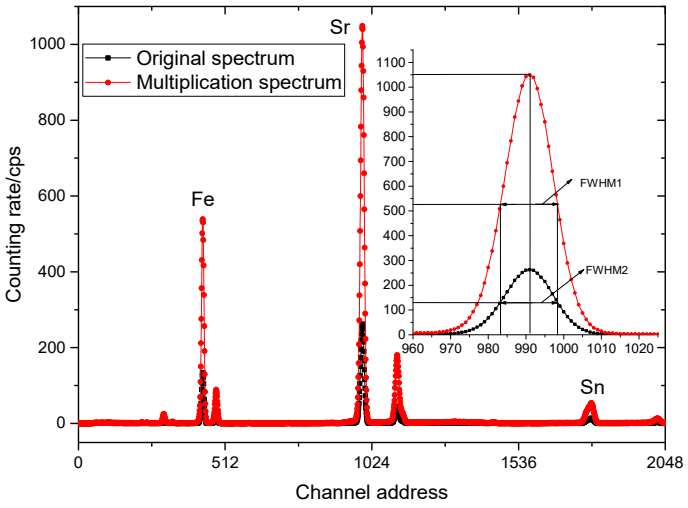

Figure 6. Comparison of the spectra before and after using the pulse circulation method.

In Figure 6, the traditional spectral method obtained the black spectral lines, whose counting rate was low. The red spectral lines were obtained by the counting multiplication method. Comparing the two figures shows that the counting rate can be doubled by using the pulse circulation method in the same measuring time.

The sum of the counting rates of the iron element, strontium element, and tin element in the corresponding range of channel address was selected as the object of comparison, and the measurement results are shown in Table 1. In the sampling process, the sample pool adopted the dynamic updating method of left-in-right-out to ensure a sufficient sample number, and the random number used in each sampling strictly obeyed the uniform distribution. Only in this way can the probability of each pulse amplitude sample being extracted be ensured to be approximately equal. Finally, the sum of the counting rates of each element in the spectrum can be multiplied equally. Table 1 compares the counting rates of the three elements before and after multiplication. Here, $C_{original}$ represents the sum of the counting rates in the original spectrum, and $C_{multiplication}$ represents the sum of the counting rates in the spectrum obtained using the pulse circulation method.

Table 1. Comparison of counting rates before and after multiplication. (Only the pulse circulation method is used).

Element Type	Channel Address	$C_{original}$	$C_{multiplication}$	$C_{multiplication}/C_{original}$
Fe	384–512	1754.67	7005.74	399.26%
Sr	896–1152	5240.53	20,940.77	399.59%
Sn	1728–1856	419.11	1656.21	395.17%
-	1-2048	8082.93	32,277.23	399.32%

5.2. FMPS Algorithm Superposition Pulse Circulation Method

Due to the limited space, this paper does not elaborate on the principle and implementation process of FMPS in detail and only gives the experimental results for comparing the change in the counting rate before and after using the pulse circulation method.

In Figure 7, the black spectral lines were obtained using the traditional spectral method, whose FHWM is marked as $FHWM_{original}$, while the red spectral lines were obtained by the FMPS algorithm, whose FHWM is marked as $FHWM_{FMPS}$; $FHWM_{FMPS}$ is less than $FHWM_{original}$. In other words, the energy resolution of the spectrum obtained by FMPS is

higher than that of the original spectrum. On the other hand, it is easy to see from Figure 7 that the counting rate of the spectrum obtained by the FMPS algorithm is lower than that of the original spectrum.

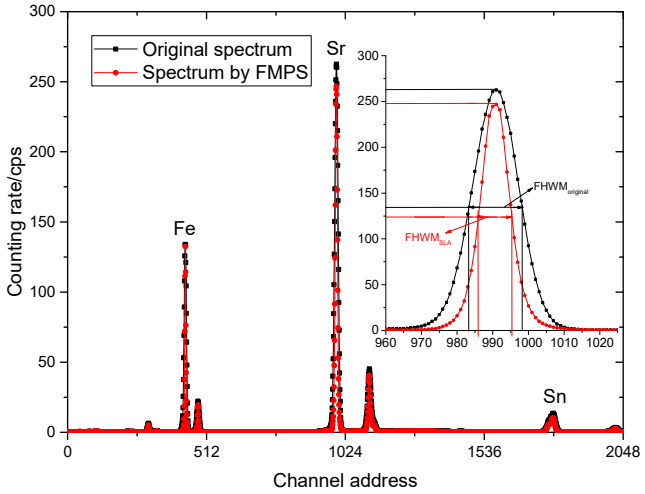

Figure 7. Comparison of the spectra before and after using FMPS.

In this section, the FMPS algorithm was superimposed on the pulse circulation method to observe the repair effect of the pulse circulation method on the loss of counting rate caused by the FMPS algorithm. Two spectra were obtained in the same measuring time before and after the multiplication method.

In Figure 8, the black spectral lines were obtained using the traditional spectral method, whose counting rate is low; the FMPS algorithm obtained the blue spectral lines. The FWHM of the blue lines is smaller than that of the black lines. That is to say, the blue spectral line has a better energy resolution than the black spectral lines. The red spectral lines were obtained by the FMPS algorithm superposition of the pulse circulation method. By comparing the three spectral lines, it can be seen that the FMPS algorithm can sharpen spectral peaks and improve energy resolution, but it also has count rate loss, which can be compensated by the pulse circulation method.

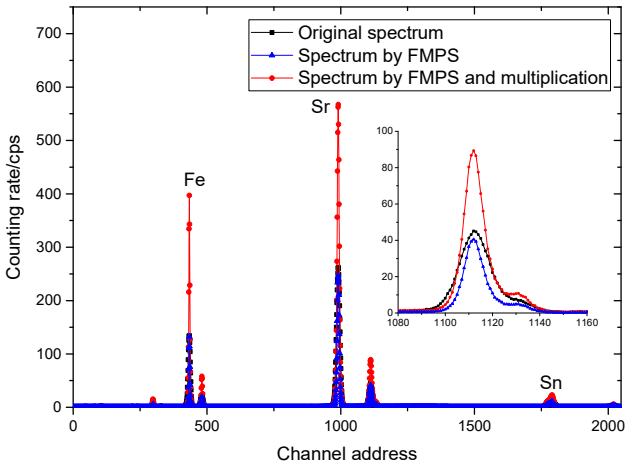

Figure 8. Comparison of the spectra obtained by different algorithms.

The sum of the counting rates of iron, strontium, and tin in the corresponding range of channel address was selected as the object of comparison, and the measurement results are shown in Table 2, which shows the comparison result of the counting rates of the three elements by different methods. Here, $C_{original}$ represents the sum of the counting rates in the spectrum without FMPS and the pulse circulation method; C_{FMPS} represents

the sum of the counting rates in the spectrum by FMPS; and $C_{repaired}$ stands for the sum of the counting rates in the spectrum by FMPS and the pulse circulation method. From Table 2, it can be concluded that although FMPS has lost a part of the counting rate while improving the energy resolution, the counting rate can be repaired using the pulse circulation method. After repairing, the sum of the counting rate was about 1.36 times that of the original spectrum.

Table 2. Comparison of the counting rates before and after multiplication. (The pulse circulation method and the FMPS algorithm are used at the same time).

Element Type	Channel Address	$C_{original}$	C_{FMPS}	$C_{repaired}$	$C_{repaired}/C_{original}$
Fe	384–512	1754.67	811.62	2433.86	138.71%
Sr	896–1152	5240.53	3254.26	7210.76	137.59%
Sn	1728–1856	419.11	252.61	555.68	132.59%
-	1–2048	8082.93	4669.81	11,029.08	136.45%

6. Discussion

Although the count rate multiplication effect can be more obvious by adjusting the sampling frequency of the pulse circulation method, considering that the process of amplitude manipulation is similar to using a filter to improve the resolution of the spectrum, the filter can steepen the steep slope in the spectrum. This filtering program is not used in gamma-ray energy spectrum analysis because it does not introduce lost information. Besides improving the resolution, it also increases the noise because the statistical fluctuation is a weak peak. In addition, if high-frequency sampling is used in limited samples, the statistical independence of the channel content will be destroyed, and the uncertainty calculation will be complicated. Therefore, the current application of the pulse circulation method is limited to repairing the lost count rate and cannot be used to improve the count rate infinitely.

7. Conclusions

In some applications, the energy characteristic peak cannot be completely separated when the semiconductor detector with the best energy resolution is used. In this case, as described in this paper, it is of great significance to propose new pulse processing and spectral methods to improve the energy resolution of the measurement system.

This paper presented a pulse circulation method implemented by a random number generator, a sample pool, and an RPC. The analog-to-digital conversion unit composed of high-precision ADC converted the analog signal into a digital negative exponential pulse signal sequence, which was stored in the dynamic sample pool. The random number generator addressed a fixed storage unit in the sample pool according to the random variables between 1 and 4096. The amplitude sample was extracted and stored in the RPC, and finally, the counting rate of the energy spectrum was multiplied.

The measurement results showed that the pulse circulation method can effectively improve the counting rate. Through the simulation and experiment, we can draw the following conclusions:

(1) The pulse circulation method can effectively multiply the counting rate and ensure that the energy resolution is not decreased.
(2) Although FMPS loses a part of the counting rate while improving the energy resolution, the counting rate can be repaired using the pulse circulation method.

Author Contributions: Conceptualization, L.T. and K.S.; methodology, L.T.; software, L.T.; validation, L.T. and S.Y.; formal analysis, S.Y.; investigation, L.T.; resources, L.T.; data curation, L.T.; writing—original draft preparation, L.T.; writing—review and editing, L.T.; visualization, L.T.; supervision, L.T.; project administration, L.T.; funding acquisition, L.T. All authors have read and agreed to the published version of the manuscript.

Funding: This work was supported by the Sichuan Natural Science Youth Fund Project (No. 2023NSFSC1366 and 23ZDYF0645), the Open Research Fund of National Engineering Research Center for Agro-Ecological Big Data Analysis & Application, Anhui University (No. AE202209), the Open Research Fund Program of Data Recovery Key Laboratory of Sichuan Province (Grant No. DRN2103), and the Research Fund of Guangxi Key Lab of Multi-source Information Mining & Security (MIMS22-04).

Data Availability Statement: Not applicable.

Acknowledgments: The authors thank Sichuan XSTAR Technology of M&C Co. Ltd, which provided the experimental platform.

Conflicts of Interest: The authors declare no conflict of interest.

Abbreviations

MCA	Multi-channel pulse height analyzer
SSPS	Simple single-pulse spectrum
FMPS	Fast multi-pulse spectrum
RPC	Random pulse circulator
FPGA	Field-programmable gate array
FIFO	First-in-first-out
CLK	Clock
ADC	Analog-to-digital converter
FWHM	Full width at half maximum
Fe	Ferrum
Sr	Strontium
Sn	Stannum

References

1. Meza Ramirez, C.A.; Greenop, M.; Ashton, L.; Rehman, I.U. Applications of machine learning in spectroscopy. *Appl. Spectrosc. Rev.* **2021**, *56*, 733–763. [CrossRef]
2. Fernandes Andrade, D.; Pereira-Filho, E.R.; Amarasiriwardena, D. Current trends in laser-induced breakdown spectroscopy: A tutorial review. *Appl. Spectrosc. Rev.* **2021**, *56*, 98–114. [CrossRef]
3. Zhang, D.; Zhang, H.; Zhao, Y.; Chen, Y.; Ke, C.; Xu, T.; He, Y. A brief review of new data analysis methods of laser induced breakdown spectroscopy: Machine learning. *Appl. Spectrosc. Rev.* **2020**, *57*, 89–111. [CrossRef]
4. Bertuccio, G.; Ahangarianabhari, M.; Graziani, C.; Macera, D.; Shi, Y.; Gandola, M.; Rachevski, A.; Rashevskaya, I.; Vacchi, A.; Zampa, G.; et al. X-ray Silicon Drift Detector–CMOS Front-End System with High Energy Resolution at Room Temperature. *IEEE Trans. Nucl. Sci.* **2016**, *63*, 400–406. [CrossRef]
5. Chen, E.-L.; Feng, C.-Q.; Liu, S.-B.; Ye, C.-F.; Jin, D.-D.; Lian, J.; Hu, H.-J. Readout electronics for a high-resolution soft X-ray spectrometer based on silicon drift detector. *Nucl. Sci. Tech.* **2017**, *28*, 14. [CrossRef]
6. Cooper, R.; Amman, M.; Vetter, K. High resolution gamma-ray spectroscopy at high count rates with a prototype High Purity Germanium detector. *Nucl. Instrum. Methods Phys. Res. Sect. A* **2018**, *886*, 1–6. [CrossRef]
7. Regadío, A.; Sánchez-Prieto, S.; Prieto, M.; Tabero, J. Implementation of a real-time adaptive digital shaping for nuclear spectroscopy. *Nucl. Instrum. Methods Phys. Res. Sect. A* **2014**, *735*, 297–303. [CrossRef]
8. Qin, H.; Lu, Z.; Yao, S.; Li, Z.; Lu, J. Combining Laser-Induced Breakdown Spectroscopy and Fourier-Transform Infrared Spectroscopy for the Analysis of Coal Properties. *J. Anal. At. Spectrom.* **2019**, *34*, 347–355. [CrossRef]
9. Zhou, J.-B.; Yu, J.; Wan, W.-J.; Zhao, X. Pulse Signal Processing Method, Device and User Terminal. China Patent 201810295672.8, 1 March 2022. (In Chinese).
10. Zhou, J.-B.; Wan, W.-J.; Yu, J. Signal Processing Method, Device and User Terminal. China Patent 2018 10090267.2, 15 June 2021. (In Chinese).
11. Tang, L.; Yu, J.; Zhou, J.; Fang, F.; Wan, W.; Yao, J.; Yu, S.; Liao, X. A new method for removing false peaks to obtain a precise X-ray spectrum. *Appl. Radiat. Isot.* **2018**, *135*, 171–176. [CrossRef] [PubMed]
12. Tang, L.; Zhou, J.; Fang, F.; Yu, J.; Hong, X.; Liao, X.; Zhou, C.; Yu, S. Counting-loss correction for X-ray spectra using the pulse-repairing method. *J. Synchrotron Radiat.* **2018**, *25*, 1760–17678. [CrossRef] [PubMed]
13. Lin, T.; Wei-Dong, Z.; Song-Ke, Y.; Ze, L.; Xiao-Dong, Y.; Yuan, M.; Xing-Lu, H. Optimization design of X-ray spectrum data processing platform. *Spectrosc. Spectr. Anal.* **2021**, *41*, 763–3767.
14. Tang, L.; Zhang, J.; Shi, K.; Liu, B.; Liu, X.; Zhao, Y.; Li, Y.; Liao, X.; Liu, Z.; Yu, S.; et al. Application of an Improved Seeds Local Averaging Algorithm in X-ray Spectrum. *Math. Probl. Eng.* **2021**, *2021*, 5545818. [CrossRef]
15. Shi, K.; Wang, J.; Tang, Y.; Zhong, S. Reliable asynchronous sampled-data filtering of T-S fuzzy uncertain delayed neural networks with stochastic switched topologies. *Fuzzy Sets Syst.* **2020**, *381*, 1–25. [CrossRef]

16. Shi, K.; Wang, J.; Zhong, S.; Tang, Y.; Cheng, J. Non-fragile memory filtering of T-S fuzzy delayed neural networks based on switched fuzzy sampled-data control. *Fuzzy Sets Syst.* **2020**, *394*, 40–64. [CrossRef]
17. Shi, K.; Tang, Y.; Zhong, S.; Yin, C.; Huang, X.; Wang, W. Nonfragile asynchronous control for uncertain chaotic Lurie network systems with Bernoulli stochastic process. *Int. J. Robust Nonlinear Control* **2018**, *28*, 1693–1714. [CrossRef]
18. Cai, X.; Zhong, S.; Wang, J.; Shi, K. Robust H∞ control for uncertain delayed T-S fuzzy systems with stochastic packet dropouts. *Appl. Math. Comput.* **2020**, *385*, 125432. [CrossRef]
19. Yu, G.-G. Research on Intelligent High Radioactive Nuclear-like Signal Generator System. Ph.D. Thesis, Chengdu University of Technology, Chengdu, China, 2017. (In Chinese).
20. Wang, M.; Zhou, J.; Hong, X.; Liu, Y. Research of single pulse trapezoidal shaping algorithm in digital nuclear spectrum measurement. *J. Comput. Theor. Nano Sci.* **2016**, *13*, 4510–4514. [CrossRef]
21. Li, D.C.; Ren, Z.G.; Yang, L.; Qi, Z.; Meng, X.T.; Hu, B.T. A novel acquisition method for nuclear spectra based on pulse area analysis. *Chin. Phys. C* **2015**, *39*, 67–70. [CrossRef]